Ann. Geophys. Discuss., https://doi.org/10.5194/angeo-2019-10
Manuscript under review for journal Ann. Geophys.
Discussion started: 5 March 2019

Annales Geophysicae Discussions

The research on small-scale structures of ice particle density and electron density in the mesopause region

Ruihuan Tian [1,2], Jian Wu[2], Jinxiu Ma[3], Yonggan Liang [1,2], Hui Li [1, 2], Chengxun Yuan[1, 4], Yongyuan Jiang[1] and Zhongxiang Zhou[1, 4]

[1]Department of Physics, Harbin Institute of Technology, Harbin 150001, China

[2]National Key Laboratory of Electromagnetic Environment (LEME), China Research Institute of Radio Wave Propagation, Beijing 102206, China

[3]CAS Key Laboratory of Geospace Environment and Department of Modern Physics, University of Science and Technology of China, Hefei 230026, China

[4] Center of Space Environment of Polar Regions, Harbin Institute of Technology, Harbin 150001, China

Correspondence to: Chengxun Yuan (yuancx@hit.edu.cn) and Hui Li (lihui_2253@163.com)

Abstract. In this paper, a growth and motion model is developed to investigate the evolution of radius, velocity, and number density of ice particles in mesopause region. In the growth model, meteoric dust from outer atmosphere and grains moving with the upward neutral wind from the mesosphere bottom serve as nuclei upon which water vapor can condense in the cold and moist condition. And the motion of the ice particles is mainly controlled by the gravity and the neutral drag force. It is shown that the radius of ice particles increases linearly with time. But the particle velocity has a complicated relationship with the radius due to the different mass densities of condensation nuclei and absorbed ice. For certain condensation core radius, the velocity of particles can be reversed at particular height, which leads to local gathering of particles near the boundary layer and small-scale structures of ice particle density on the order of a few meters. Based on the obtained small-scale ice particle distribution, the mean particle charge number and corresponding distributions of electrons are calculated by combining the dust charging processes and quasi-neutrality condition. It shows that the absorption of electrons by ice particles results in the formation of small-scale electron density structures, which can be important to the research on the cause of polar mesosphere summer echoes (PMSE).

1 Introduction

The polar mesosphere summer echoes (PMSE) are strong radar echoes from regions close to the polar mesopause in summer(Rapp and Lübken 2004). One of the features of PMSE is that the spectra widths

Ann. Geophys. Discuss., https://doi.org/10.5194/angeo-2019-10
Manuscript under review for journal Ann. Geophys.
Discussion started: 5 March 2019

of echoes are much narrower than that of incoherent scatter (being due to the Brownian movement of electrons)(Röttger, et al. 1988;Röttger, et al. 1990). And it has been proposed that the PMSEs are radar waves coherently scattered by the irregularities of the refractive index that are mainly determined by electron density(Rapp and Lübken 2004). Furthermore, the efficient scattering occurs when the spatial scale of electron density structures is half the radar wavelength, the so-called Bragg scale. For typical VHF radars, the scale is about 3 m(Rapp and Lübken 2004). Experimentally, in the ECT02 campaign(Lübken, et al. 1998), the sounding rocket with electron probe has detected electron density irregularities on the order of meters during the simultaneous observation of PMSE, which provides a vital argument for that small-scale electron density structures can indeed create strong radar echoes. However, the mechanism that gives rise to the observed small-scale electron density structures has not been fully understood.

Lots of researches indicate that charged ice particles in the PMSE region play a key role in creating small-scale structures of electron density(Antonsen, et al. 2017;Havnes, et al. 2015;Lübken, et al. 2009;Li, et al. 2016;Rapp and Lübken 2004;Rapp and Lübken 2003;Ullah, et al. 2018). The measured temperature in the polar mesopause region is lower than the freezing point(Körner and Sonnemann 2001;Lübken, et al. 2009), and the environment there is moist enough(Lübken 1999). These two elements allow the presence of ice particles between 80 and 90 km, and the adsorption of electrons by ice crystals can result in a decrease in electron density. Experimentally, large local gradients in ice particle density have been detected and an anticorrelation between electron density and ice particle charge density is found under the PMSE condition(Havnes, et al. 1996). Moreover, if the observation region is heated by radio frequency at high power, the PMSE can be weakened with the ice on particle surface sublimating(Chilson, et al. 2000;Havnes, et al. 2015). The ice particles are much heavier than ions and electrons(Reid 1990), So the particle mobility is very small and the small-scale structures of ice particle distribution can stay for a relatively long time. This may be one of the reasons why the PMSE can last for several hours(Ecklund and Balsley 1981).

The influence of imposed small-scale ice particle density structures on the mesopause plasma has been studied by Ø. Lie-Svendsen et al(Lie‐Svendsen, et al. 2003). The results show that irregular ice particle density on the order of meters can cause similar small-scale electron density structures, which could produce PMSE. But the origin of such small-scale ice particle irregularities is not clear.

Ann. Geophys. Discuss., https://doi.org/10.5194/angeo-2019-10
Manuscript under review for journal Ann. Geophys.
Discussion started: 5 March 2019

Annales Geophysicae Discussions

In this work, we try to investigate the formation of small-scale ice particle density structures from the perspective of particle growth and motion, and then calculate their influence on electron density by a charging model. The growth of particles is based on collision and adsorption process of water vapor and condensation nuclei. The particle movement is mainly controlled by the gravity and the neutral drag force. And the charging model comprises orbital motion limited (OML) theory, collision enhanced collection (CEC) approximation, and quasi-neutrality condition.

2 Model

In this section the equations of the growth and motion model of condensation nuclei and the charging model of ice particles are described.

The simulation is carried out at summer polar mesopause region between 80 ~ 90 km, where the water vapor carried by neutral gas is supposed to move upwards at a constant speed(Garcia and Solomon 1985). To simplify the calculation procedure, we assume that micrometeorites enter the region at a certain flux from the upper boundary, and volcanic ash or particles ejected by aircraft rise into the region from the lower boundary. These grains serve as condensation cores. With the temperature lower than the frost point(Körner and Sonnemann 2001), the water vapor molecules that touch the surface of the grains due to thermal motion can easily condense into ice, which makes condensation cores become ice particles and keep growing. Meantime, only vertical transport of particles and plasma is considered in this paper, because the horizontal gradients of transport parameters are much smaller than the vertical ones(Lie‐Svendsen, et al. 2003).

For growing ice particles, the dynamic equation for variable mass object is applied:

$$m_{\mathrm{d}} \frac{\mathrm{d}\boldsymbol{v}_{\mathrm{d}}}{\mathrm{d}t} + (\boldsymbol{v}_{\mathrm{d}} - \boldsymbol{u}) \frac{\mathrm{d}m_{\mathrm{d}}}{\mathrm{d}t} = m_{\mathrm{d}}\boldsymbol{g} - \mu_{\mathrm{dn}} m_{\mathrm{d}} (\boldsymbol{v}_{\mathrm{d}} - \boldsymbol{u}) + q_{\mathrm{d}}\boldsymbol{E} \qquad (1)$$

where m_{d}, $\boldsymbol{v}_{\mathrm{d}}$ and q_{d} are the mass, velocity, and charge of ice particles respectively. $\boldsymbol{u}$ is the velocity of neutral gas; $\boldsymbol{g}$ is the gravitational acceleration; μ_{dn} is the collision frequency between ice particles and gas; and $\boldsymbol{E}$ is the electric field. The electric force has trivial effect on the motion of ice particles, because the charge-mass ratio of particles is usually very small(Jensen and Thomas 1988;Pfaff, et al. 2001).

The first term on the left side of Eq. (1) corresponds to the inertial term. The vertical wind speed and ice particles speed v_{d} in the mesospause are several centimeters per second(Garcia and Solomon 1985). The spatial scale of PMSE layer L is several meters to kilometers. Then the range of magnitude of term

Ann. Geophys. Discuss., https://doi.org/10.5194/angeo-2019-10
Manuscript under review for journal Ann. Geophys.
Discussion started: 5 March 2019

Annales Geophysicae Discussions

inertial term is estimated as

$$\frac{dv_d}{dt} \sim \frac{v_d}{\tau} \sim \frac{v_d^2}{L} \sim (10^{-7}\text{m/s}^2\text{-}10^{-2}\ \text{m/s}^2) \ll g \quad (2)$$

Therefore, the inertial effect of ice particles during motion is not important and can be ignored.

The second term on the left side of Eq. (1) represents the mass change caused by water vapor collection. We assume that all water molecules colliding with ice particles during thermal motion can condense on them because the water vapor is oversaturated(Lübken 1999). Ignoring reverse process such as sublimation, the mass change rate for ice particles is

$$\frac{dm_d}{dt} = \mu_{wd} m_w \quad (3)$$

where μ_{wd} is the collision frequency, and m_w is the mass of water molecule. Since the thermal velocity of water vapor v_w is usually much larger than particle velocity v_d and the ice particle radius r_d is much larger than the water molecule radius r_w, the collection frequency μ_{wd} can be approximately deduced as the following Eq. (4) based on the hard-sphere collision model(Lieberman and Lichtenberg 2005).

$$\mu_{wd} = n_w \pi r_d^2 v_w \quad (4)$$

The second term on the right side of Eq. (1) is the neutral drag force. The collision frequency between air molecules and ice particles is(Schunk 1977)

$$\mu_{dn} = \frac{8}{3\sqrt{\pi}} \frac{n_n m_n}{m_d + m_n} \sqrt{\frac{2k_B T_g (m_d + m_n)}{m_d m_n}} \pi (r_d + r_n)^2 \quad (5)$$

where n_n, m_n, and r_n are number density, mean molecule mass, and effective radius of neutral molecule, respectively. T_g is the gas temperature. Due to $m_d >> m_n$, and $r_d >> r_n$

$$\mu_{dn} \approx \frac{4}{3} n_n \frac{m_n}{m_d} v_n \pi r_d^2 \quad (6)$$

where the thermal velocity of neutral molecule $v_n = (8k_B T_g/\pi/m_n)^{1/2}$, and the neutral molecule mass m_n is assumed as $28.96m_u$. m_u is the mass of a proton.

Combining Eq. (1) ~ (3), we can get the velocity of ice particles

$$\boldsymbol{v}_d = \boldsymbol{u} + \frac{m_d}{\mu_{dn} m_d + \mu_{wd} m_w} \boldsymbol{g} \quad (7)$$

Ann. Geophys. Discuss., https://doi.org/10.5194/angeo-2019-10
Manuscript under review for journal Ann. Geophys.
Discussion started: 5 March 2019

Annales Geophysicae Discussions

By considering the restrictions of $n_w << n_n$(Seele and Hartogh 1999), $m_w << m_d$ and $v_n \sim v_w$, and taking vertical up to be the positive direction, the velocity of ice particles is simplified as

$$v_d = u - g/\mu_{dn} \tag{8}$$

Ice particles are composed of condensation nuclei and attached ice. The mass of a single ice particle is

$$m_d = \frac{4}{3}\pi r_0^3 \rho_0 + \frac{4}{3}\pi(r_d^3 - r_0^3)\rho_d \tag{9}$$

where r_0 and ρ_0 are the initial radius and mass density of condensation nuclei, and ρ_d is the mass density of ice.

Combining Eq. (6), (8) and (9), the relationship between velocity and radius of ice particles is

$$v_d = u - \frac{g}{n_n m_n v_n}[\rho_d r_d + (\rho_0 - \rho_d)\frac{r_0^3}{r_d^2}] \tag{10}$$

At the upper and lower boundaries of PMSE layer, with $r_d = r_0$ the initial velocity of condensation nuclei is

$$v_{d0} = u(1 - r_0/r_c) \tag{11}$$

r_c is the critical radius

$$r_c = n_n m_n v_n u/(g\rho_0) \tag{12}$$

When the radius of condensation nuclei $r_0 > r_c$, gravity is larger than neutral drag force, $v_{d0} < 0$, and particles move downwards. Otherwise, particles move upwards.

Substituting Eq. (9) into Eq. (2), the change rate of ice particle radius with time is

$$\frac{dr_d}{dt} = \frac{1}{4}\frac{n_w m_w v_w}{\rho_d} = c \tag{13}$$

The growth rate of particles is a constant c related to the vapor number density. So the ice particle radius increases linearly with time

$$r_d = r_0 + ct \tag{14}$$

Based on Eq. (14), the particle trajectory can be obtained by the following integral

Ann. Geophys. Discuss., https://doi.org/10.5194/angeo-2019-10
Manuscript under review for journal Ann. Geophys.
Discussion started: 5 March 2019

Annales Geophysicae Discussions

$$z - z_0 = \int_0^t v_d \mathrm{d}t = c^{-1} \int_{r_0}^{r_d} v_d \mathrm{d}r_d \tag{15}$$

z_0 is the reference height where condensation nuclei enter the studied region. It is set that $z_0 = 0$ for the lower boundary and $z_0 = h$ for the upper one, here h is the distance between the two boundaries.

We assume that the condensation nucleus radius ranging from $r_{0\min}$ to $r_{0\max}$ has a certain distribution function $f(r_0)$. The density of condensation nuclei with radius in a small scale $r_0 \rightarrow r_0 + \mathrm{d}r_0$ is $\mathrm{d}n(r_0) = f(r_0)\,\mathrm{d}r_0$, and their velocity is v_{d0}. When these particles arrive at height z, their radius increases to $r_d(r_0, z)$, the corresponding number density turns into $\mathrm{d}n(r_0, z)$, and the velocity becomes $v_d(r_0, z) = v_d[r_0, r_d(r_0, z)]$. According to the particle-conservation law, we have

$$v_{d0}\mathrm{d}n(r_0) = v_d(r_0, z)\mathrm{d}n(r_0, z) \tag{16}$$

Then the number density of ice particles at height z can be obtained by

$$n_d(z) = \int \mathrm{d}n(r_0, z) = \int_{r_{0\min}}^{r_{0\max}} \frac{v_{d0} f(r_0)}{v_d(r_0, z)} \mathrm{d}r_0 \tag{17}$$

The average ice particle radius can also be described by the distribution function $f(r_0)$

$$\overline{r}_d(z) = \frac{\int r_d(z)\mathrm{d}n(r_0, z)}{n_d(z)} \tag{18}$$

Then the electron density can be calculated based on the dust charging processes and the quasi-neutrality condition. Based on the plasma and ice particle characteristics studied in this paper, the OML theory(Allen 1992) and CEC approximation(Khrapak, et al. 2005) are employed to describe the electron and ion charging processes respectively. The corresponding ion charging currents are

$$I_e = -4\pi r_d^{\,2} n_e e \left(\frac{k_B T_e}{2\pi m_e}\right)^{1/2} \exp\left(\frac{e\varphi_d}{k_B T_e}\right) \tag{19}$$

$$I_i = 4\pi r_d^{\,2} n_i e \left(\frac{k_B T_i}{2\pi m_i}\right)^{1/2} \left[1 - \frac{e\varphi_d}{k_B T_i} + 0.1\left(\frac{e\varphi_d}{k_B T_i}\right)^2 \frac{\lambda_D}{l_i}\right] \tag{20}$$

where n_e, m_e, and T_e are the density, mass, and temperature of electrons. In the typical PMSE layer, there are several kinds of ions carrying one unit positive charge: N_2^+, O_2^+, NO^+ and $H^+(H_2O)_n$. For simplifying the calculation, the averaged ion parameters n_i, m_i, and T_i are applied to describe the density, mass, and temperature of ions respectively. According to Ref. (Reid 1990), $m_i = 50m_u$. φ_d is the surface

Ann. Geophys. Discuss., https://doi.org/10.5194/angeo-2019-10
Manuscript under review for journal Ann. Geophys.
Discussion started: 5 March 2019

potential of charged ice particles, λ_D is the plasma Debye length, and temperature $T_e = T_i = T_g$.

For spherical particles, the surface potential φ_d is

$$\varphi_d = -\frac{Z_d e}{4\pi\varepsilon_0 r_d} \tag{21}$$

where Z_d is the charge number of single ice particle. The radius of ice particles r_d can be represented by $\bar{r}_d$ obtained above.

During the growth and movement of ice particles, the charging balance of ice particles is maintained:

$$I_i + I_e = 0 \tag{22}$$

According to the typical parameters in PMSE region(Rapp and Lübken 2001), the plasma Debye length λ_D is estimated to be about 9 mm, which is much smaller than the vertical spatial scale of PMSE layer. So the dusty plasma satisfies the quasi-neutral condition:

$$n_e + Z_d n_d = n_i \tag{23}$$

To analyze the influence of ice particles on the electron density distribution more simply, the ion density n_i is assumed to remain unchanged (the empirical value is 6×10^9 m^{-3}) in the calculation region according to Ref.(Johannessen and Krankowsky 1972;Pedersen, et al. 1970;Reid 1990). With the n_d and r_d obtained above, the mean charge number of ice particles Z_d and electron density n_e can be calculated from Eq. (19) ~ (23).

In subsequent calculations, parameters are taken in the atmospheric environment at altitude of 85 km. The number density of neutrals $n_n = 2.3\times10^{20}$ m^{-3}(Hill, et al. 1999), the number density of water vapor $n_w = 2.5\times10^{14}$ m^{-3}(Seele and Hartogh 1999), temperature $T_g = 150$ K, the mass density of ice $\rho_d = 1\times10^3$ kg/m^3, the velocity of neutral wind $u = 3$ cm/s(Garcia and Solomon 1985), the mass density of condensation nucleus $\rho_0 = 2.7\times10^3$ kg/m^3, and the growth rate of ice particles in Eq. (14) $c \approx 7.8\times10^{-4}$ nm/s. In this work, we only consider the growth and movement of condensation nucleus which fall from the upper boundary for $r_0 > r_c$ and rise from lower boundary for $r_0 \le r_c$.

3 Results and discussion

For convenience of calculations, dimensionless parameters are used:

$$V_d = v_d/u,\quad \rho = \rho_d/\rho_0,\quad R_0 = r_0/r_c,\quad R_d = r_d/r_c$$

Ann. Geophys. Discuss., https://doi.org/10.5194/angeo-2019-10
Manuscript under review for journal Ann. Geophys.
Discussion started: 5 March 2019

$$T = t/t_c, \quad Z = (z - z_0)/z_c$$

where $t_c = r_c/c$, which represents the time it takes for ice particle radius r_d growing to r_d+r_c, and $z_c = ut_c$ is the distance that neutral wind moves during the time t_c. In this study r_c = 4.2 nm, $t_c \approx$ 5385 s, and $z_c \approx$ 161 m.

The dimensionless expression of ice particle velocity is

$$V_d = 1 - \rho R_d - (1-\rho)\frac{R_0^3}{R_d^2} \tag{24}$$

The change rate of V_d with R_d is

$$\frac{\partial V_d}{\partial R_d} = -\rho + 2(1-\rho)\frac{R_0^3}{R_d^3} \tag{25}$$

Based on Eq. (14), (15) and (24), the dimensionless expressions of ice particle position coordinate in terms of time and radius are

$$Z(R_0, T) = T - \frac{1}{2}\rho T(T + 2R_0) - (1-\rho)R_0^2\frac{T}{T + R_0} \tag{26}$$

$$Z(R_0, R_d) = R_d - R_0 - \frac{1}{2}\rho(R_d^2 - R_0^2) + (1-\rho)R_0^3\left(\frac{1}{R_d} - \frac{1}{R_0}\right) \tag{27}$$

The dependence of V_d on R_d is illustrated in Fig. 1(a). According Eq. (11) and (24), condensation nuclei with radius $R_0 \leq 1$ rise into the PMSE region through the lower boundary, while particles with initial $R_0 > 1$ fall into the region from the upper boundary. At the beginning, the upward-moving particles accelerate and the downward ones decelerate due to $\partial V_d/\partial R_d = 2 - 3\rho > 0$ for the initial $R_d = R_0$. Later, with the increase of R_d, $\partial V_d/\partial R_d < 0$, all particles will move with an acceleration less than zero, which makes them move downward eventually.

Figure 1(b) shows the movement curves of ice particles near the lower boundary. These particles rise into the condensation layer with an initial radius $R_0 \leq 1$. With the collection of ice, the grains become larger and heavier, which leads to the deceleration of the grains. And then, the grains will accelerate downward until they leave the condensation layer from the lower boundary. From Fig. 1(b) it can be seen that all particles rising from the lower boundary will retrace in the range of $Z_m < Z < Z_M$.

Ann. Geophys. Discuss., https://doi.org/10.5194/angeo-2019-10
Manuscript under review for journal Ann. Geophys.
Discussion started: 5 March 2019

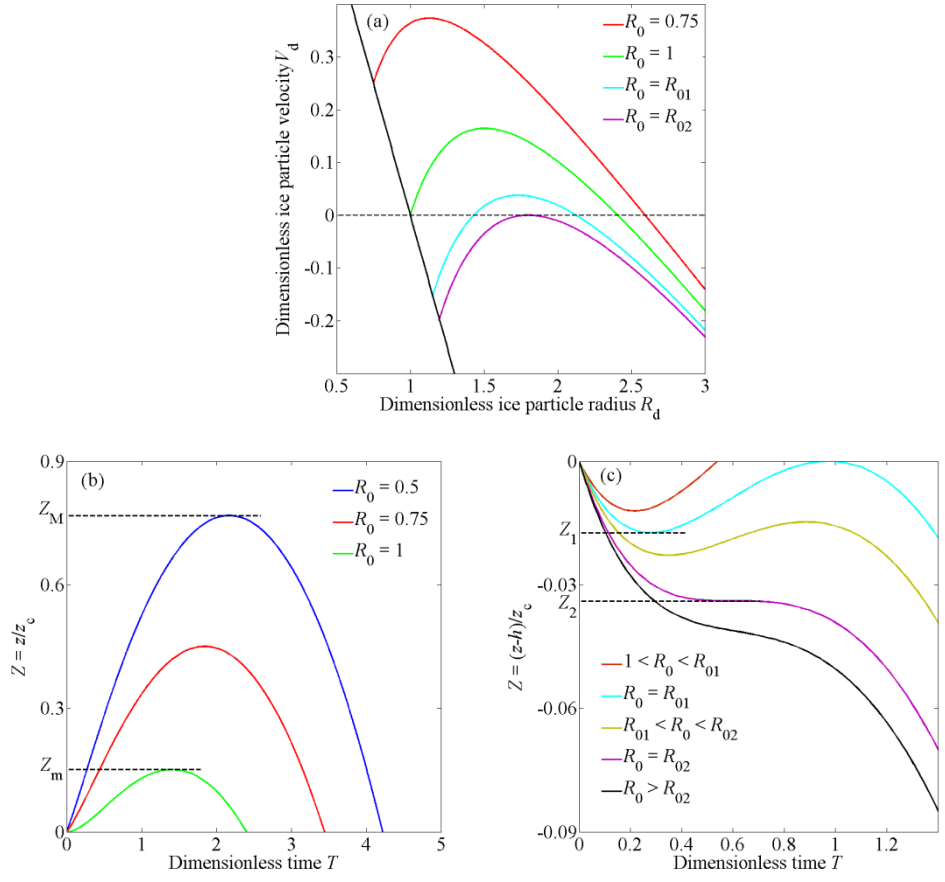

Figure 1 (a) The dependence of ice particle velocity on radius at various values of initial nucleus radii. The black solid line V_{d0} = 1- R_0 represents the collection of starting points. (b) The movement curves of ice particles near the lower boundary. (c) The movement curves of ice particles near the upper boundary. Z_m is the maximum height that particles with initial radius R_0 = 1 can rise; Z_M is the maximum height that particles with initial radius R_0 = R_{0min} = 0.5 can rise. Based on Eq. (24) and (27), Z_m = 0.1512 and Z_M = 0.7631. R_{01} and R_{02} are two critical values of condensation nucleus radius. For R_0 = R_{01} particles fall into the condensation layer, first retrace at height Z_1, and then retrace exactly at the upper boundary. When R_0 = R_{02}, the particles move down to the height Z_2, the velocity and acceleration are exactly zero, and then they continue to move down. According to Eq. (24), (25), and (27), R_{01} = 1.1519 and R_{02} = 1.19705.

Figure 1(c) shows the movement curves of ice particles near the upper boundary. The condensation cores fall into the cold layer with radius R_0 > 1. The movement curves of these particles can be sorted

Ann. Geophys. Discuss., https://doi.org/10.5194/angeo-2019-10
Manuscript under review for journal Ann. Geophys.
Discussion started: 5 March 2019

by the value of R_0. For $1 < R_0 < R_{01}$, the neutral drag force increases faster than the gravity as the particles fall. The particles decelerate to zero speed, and then retrace upward until they leave the condensation layer from the upper boundary. For $R_0 = R_{01}$, the particles retrace at the height $Z = Z_1$. Then they arrive at $Z = 0$ with exactly zero velocity, and the particles move back into the condensation layer again. For $R_{01} < R_0 < R_{02}$, the particles retrace upward in the range of $Z_2 < Z < Z_1$ and move downward again before they arrive at the upper boundary. For $R_0 = R_{02}$, the particles decelerate downward until zero speed at $Z = Z_2$. Here, the acceleration happens to be zero. Then the gravity exceeds the drag force, and the particles accelerate downward. For $R_0 > R_{02}$, the particles keep going down after entering the condensation layer without turning back.

From Fig. 1, it is concluded that the particles with a certain range of initial radius will move up and down for a few times near the boundary, namely, ice particles will accumulate at that region and form some kind of small-scale density structure.

The dimensionless expressions of ice particle number density can be obtained from Eq. (17)

$$n_{\mathrm{d}}(Z) = n_0 \int_{R_{0\min}}^{R_{0\max}} \frac{V_{\mathrm{d}0} F(R_0)}{V_{\mathrm{d}}[R_0, R_{\mathrm{d}}(R_0, Z)]} \mathrm{d}R_0 \tag{28}$$

where n_0 is the density of condensation cores at the boundary, and n_0 is assumed to be 1×10^9 m^{-3}(Bardeen, et al. 2008). The normalized radius distribution function $F(R_0)$ satisfies

$$\int_{R_{0\min}}^{R_{0\max}} F(R_0)\,\mathrm{d}R_0 = 1 \tag{29}$$

Combining Eq. (18) and (28) the dimensionless average radius of ice particles is

$$\bar{R}_{\mathrm{d}}(Z) = \frac{n_0}{n_{\mathrm{d}}(Z)} \int_{R_{0\min}}^{R_{0\max}} \frac{R_{\mathrm{d}}(Z) V_{\mathrm{d}0} F(R_0)}{V_{\mathrm{d}}[R_0, R_{\mathrm{d}}(R_0, Z)]} \mathrm{d}R_0 \tag{30}$$

Firstly, the density and radius distributions of ice particles rising into the condensation layer through the lower boundary are discussed. It is shown in Fig. 1(b) that all ice particles with initial radius $R_0 \le 1$ will pass the range $0 < Z < Z_{\mathrm{m}}$ twice, so they contribute twice to the calculation of particle density. And in the height range $Z_{\mathrm{m}} < Z < Z_{\mathrm{M}}$, only the particles that retrace above the Z height can contribute to the density calculation at Z. Then the expressions of their density and mean radius near the lower boundary can be obtained from Eq. (28) and (30)

Ann. Geophys. Discuss., https://doi.org/10.5194/angeo-2019-10
Manuscript under review for journal Ann. Geophys.
Discussion started: 5 March 2019

Annales Geophysicae Discussions
Open Access
EGU

$$n_{\mathrm{d}}(Z) = n_0 \int_{0.5}^{R_{0Z}} V_{\mathrm{d}0} F(R_0) \left[\frac{1}{V_{\mathrm{d}1}(R_0, R_{\mathrm{d}1})} + \frac{1}{|V_{\mathrm{d}2}(R_0, R_{\mathrm{d}2})|} \right] \mathrm{d}R_0 \tag{31}$$

$$\bar{R}_{\mathrm{d}}(Z) = \frac{n_0}{n_{\mathrm{d}}(Z)} \int_{0.5}^{R_{0Z}} V_{\mathrm{d}0} F(R_0) \left[\frac{R_{\mathrm{d}1}}{V_{\mathrm{d}1}(R_0, R_{\mathrm{d}1})} + \frac{R_{\mathrm{d}2}}{|V_{\mathrm{d}2}(R_0, R_{\mathrm{d}2})|} \right] \mathrm{d}R_0 \tag{32}$$

$R_{\mathrm{d}1}$ and $R_{\mathrm{d}2}$ are particle radii when particles pass through the Z height, and they can be calculated from Eq. (27); $V_{\mathrm{d}1}$ and $V_{\mathrm{d}2}$ are their corresponding velocities, which can be calculated by Eq. (24); as for the upper limit of integral R_{0Z}, it can be determined by

$$R_{0Z} = \begin{cases} 1 & \text{if } 0 < Z < Z_{\mathrm{m}} \\ \text{solution of } \left(Z\left(R_{0Z}, R_{\mathrm{d}}\right) = Z \right) & \text{if } Z_{\mathrm{m}} < Z < Z_{\mathrm{M}} \end{cases} \tag{33}$$

In this study, the radius distribution function of condensation cores is assumed as Gaussian distribution

$$F(R_0) = A \exp[-(R_0 - R_{00})^2 / \Delta^2] \tag{34}$$

where the radius of the distribution function center R_{00} is chosen as 0.8, the characteristic width Δ = 0.03, and the corresponding normalized coefficient A = 18.8.

Combining Eq. (31) ~ (34), the density and mean radius of ice particles near the lower boundary are calculated, and the results are shown in Fig. 2(a) and 2(b) respectively. Figure 2(a) shows that a sharp peak appears in density distribution of ice particles at the range of 50 ~ 70 m. From Fig. 2(b), we can see that the average radius of ice particles increases from 7 nm to 10 nm with height.

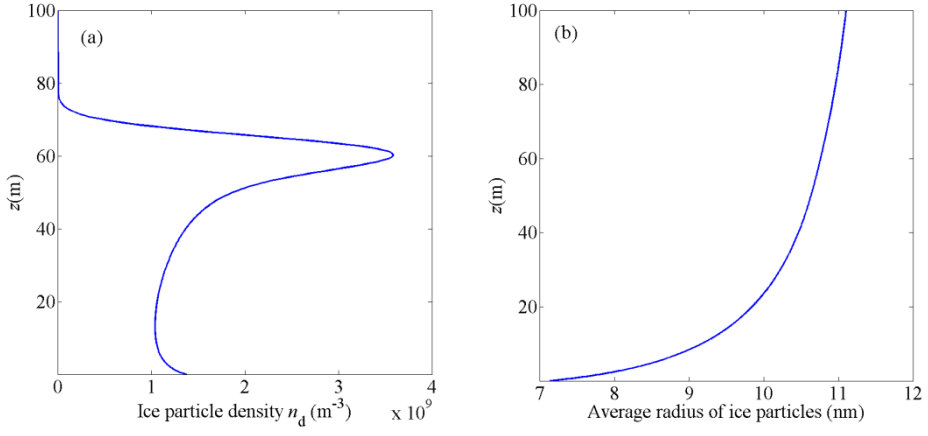

Ann. Geophys. Discuss., https://doi.org/10.5194/angeo-2019-10
Manuscript under review for journal Ann. Geophys.
Discussion started: 5 March 2019

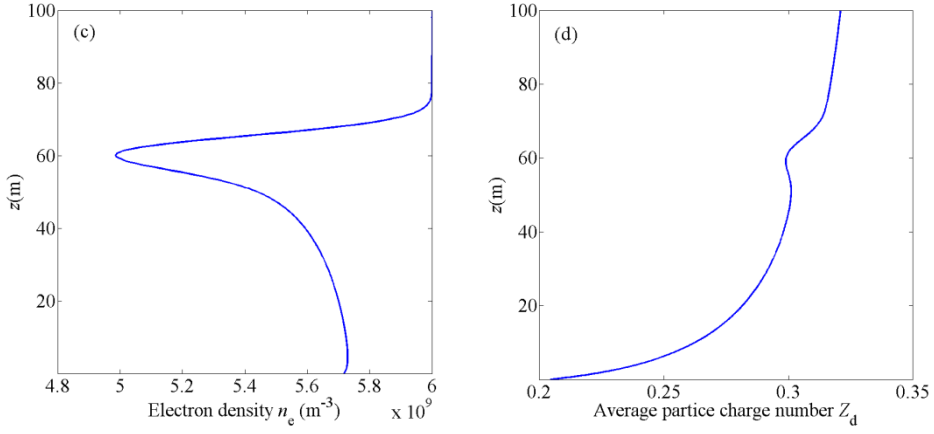

Figure 2 The distribution of (a) ice particle density, (b) mean particle radius, (c) electron density, and (d) mean charge number of ice particles near the lower boundary of condensation layer.

With the obtained density and average radius of ice particles in Fig. 2(a) and 2(b), the electron density and average charge number of ice particles are calculated based on Eq. (19) ~ (23), and the results are illustrated in Fig. 2(c) and Fig.2(d). Because of the collection of electrons by ice particles, the electron density decreases obviously in the range of 50 ~ 70 m and a small-scale structure is formed at that region. The average charge number of ice particles Z_d in Fig. 2(d) ranges from 0.2 to 0.33 and generally increases with height because the particles radius increases with height. But in the height range 50 ~ 70 m, Z_d is slightly reduced due to the dramatic increase of ice particles and decrease of electrons in this range.

Next, the parameters of ice particles and electrons near the upper boundary are discussed based on the movement curves of ice particles near the upper boundary, which are shown in Fig. 3.

Ann. Geophys. Discuss., https://doi.org/10.5194/angeo-2019-10
Manuscript under review for journal Ann. Geophys.
Discussion started: 5 March 2019

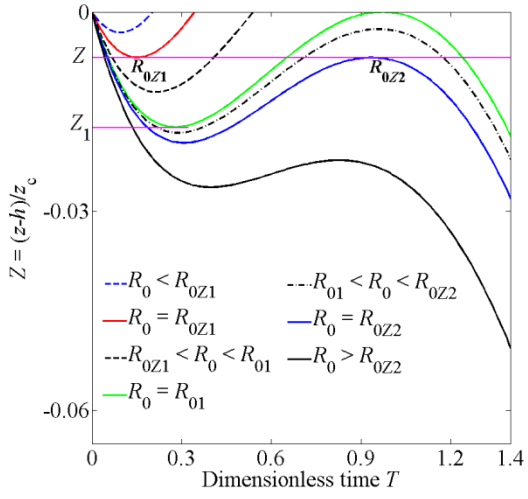

Figure 3 The movement curves of ice particles near the upper boundary. The particles with initial radius R_{0Z1} move upward after turning back at the Z height (the red line), and the particles with initial radius R_{0Z2} move downward after turning back at Z (the blue line).

For $Z_1 < Z < 0$, two kinds of particles turn back at Z: particles with initial radius R_{0Z1} and R_{0Z2}, which go upward and downward separately as shown in Fig. 3. And the values of R_{0Z1} and R_{0Z2} are determined by equations $V_d(R_{0Z}, R_d) = 0$ and $Z(R_{0Z}, R_d) = Z$. According to the range of initial radius R_0, the ice particles contribute to the density distribution near the upper boundary can be classified as follows.

(1) $R_0 < R_{0Z1}$: ice particles cannot arrive at Z and make no contributions to the number density.

(2) $R_{0Z1} < R_0 < R_{01}$: ice particles pass through Z twice and contribute to $n_d(Z)$ twice. The radius of particles passing through the Z height can be obtained as R_{d31} and R_{d32} based on Eq. (27). Meanwhile their corresponding velocities are calculated as V_{d31} and V_{d32} respectively based on Eq. (24).

(3) $R_{01} < R_0 < R_{0Z2}$: ice particles pass through Z three times. The corresponding radii and velocities at Z are defined as R_{d41}, R_{d42}, R_{d43}; V_{d41}, V_{d42}, V_{d43}.

(4) $R_0 > R_{0Z2}$: ice particles pass through Z only once and their radius and velocity are R_{d5} and V_{d5} respectively.

Substituting these parameters into Eq. (28) and (30), the density and mean radius of ice particles in the range of $Z_1 < Z < 0$ are deduced as

Ann. Geophys. Discuss., https://doi.org/10.5194/angeo-2019-10
Manuscript under review for journal Ann. Geophys.
Discussion started: 5 March 2019

Annales Geophysicae Discussions
Open Access
EGU

$$n_d(Z) = n_0 \int_{R_{0Z1}}^{R_{01}} V_{d0} F(R_0) \left[\frac{1}{|V_{d31}(R_0, R_{d31})|} + \frac{1}{V_{d32}(R_0, R_{d32})} \right] dR_0 + n_0 \int_{R_{01}}^{R_{0Z2}} V_{d0} F(R_0) \left[\frac{1}{|V_{d41}(R_0, R_{d41})|} + \frac{1}{V_{d42}(R_0, R_{d42})} + \frac{1}{|V_{d43}(R_0, R_{d43})|} \right] dR_0 + n_0 \int_{R_{0Z2}}^{R_{0max}} \frac{V_{d0} F(R_0)}{|V_{d5}(R_0, R_{d5})|} dR_0 \quad (35)$$

$$\bar{R}_d(Z) = \frac{n_0}{n_d(Z)} \int_{R_{0Z1}}^{R_{01}} V_{d0} F(R_0) \left[\frac{R_{d31}}{|V_{d31}(R_0, R_{d31})|} + \frac{R_{d32}}{V_{d32}(R_0, R_{d32})} \right] dR_0 + \frac{n_0}{n_d(Z)} \int_{R_{01}}^{R_{0Z2}} V_{d0} F(R_0) \left[\frac{R_{d41}}{|V_{d41}(R_0, R_{d41})|} + \frac{R_{d42}}{V_{d42}(R_0, R_{d42})} + \frac{R_{d43}}{|V_{d43}(R_0, R_{d43})|} \right] dR_0 + \frac{n_0}{n_d(Z)} \int_{R_{0Z2}}^{R_{0max}} \frac{R_{d5} V_{d0} F(R_0)}{|V_{d5}(R_0, R_{d5})|} dR_0 \quad (36)$$

where the radius distribution function of condensation cores $F(R_0)$ are set to satisfy the Gaussian distribution as described by Eq. (34) with the distribution function center R_{00} = 1.08, the characteristic width Δ = 0.01, and the corresponding normalized coefficient A = 56.4.

The ice particle density in the range of $Z < Z_1$ is close to zero, since only particles with initial radius $R_0 \geq R_{01}$ can arrive at the range and the number of particles in this radius range is very few based on the parameters of $F(R_0)$ set above.

At the upper boundary, the number density of condensation cores n_0 is set as 1×10^9 m^{-3}; the maximum radius of condensation cores R_{0max} = 1.3. The number density and mean radius of ice particles are obtained from Eq. (35) and (36). And based on Eq. (19) ~ (23) the electron density and mean charge number of ice particles are calculated further. The results are shown in Fig. 4. The distribution of ice particle density has a thin layer structure of meters, which leads to the same but anti-correlated structure for electrons. As shown in Fig. 2(c) and Fig. 4(c), the spatial scale of the sharp boundary in electron density distribution is on the order of tens of centimeters to several meters, which is similar to the spatial scale required for PMSE(Rapp and Lübken 2004).

Ann. Geophys. Discuss., https://doi.org/10.5194/angeo-2019-10
Manuscript under review for journal Ann. Geophys.
Discussion started: 5 March 2019

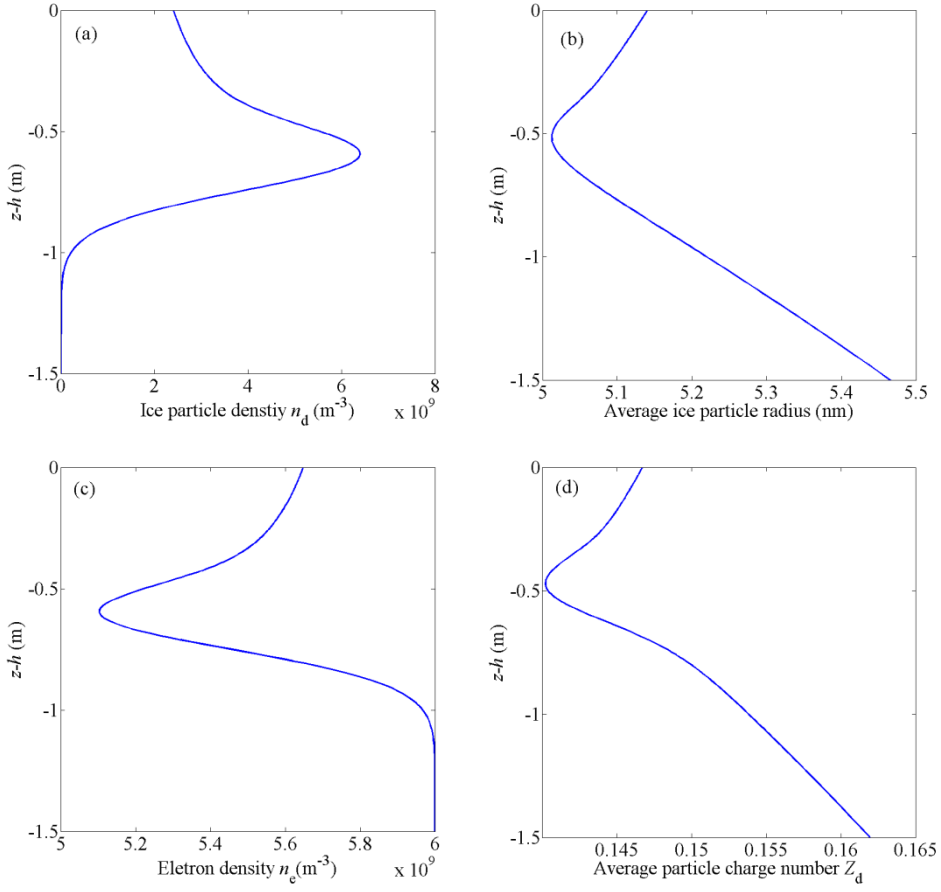

Figure 4 The distribution of (a) ice particle density, (b) mean particle radius, (c) electron density, and (d) mean charge number of ice particles near the upper boundary of condensation layer.

4 Conclusion

In summary, the density distribution of ice particles and electrons near the boundary of PMSE region is studied. Firstly, a growth and motion model of ice particles is developed based on the adsorption effect of water vapor by particles and dynamic equation for variable mass object. Then the density of ice particles with height is investigated according to the conservation of particle number. Finally, on the basis of quasi-neutrality and a charging model consisting of OML theory and CEC approximation, the corresponding electron density distribution is obtained. During the calculation, the parameters are chosen under the atmospheric environment at an altitude of 85 km, where PMSEs are often detected.

The results show that the ice particle radius increases linearly with time. But due to the different mass

densities of condensation nuclei and absorbed ice, there is a complex relationship between the velocity and radius of particles. So for a certain range of the condensation core radius, particles can bounce and locally gather somewhere. When the radius distribution function of condensation nucleus is Gaussian type, sharp peaks with scale of meters appear in the ice particle density profile. Because of the absorption by ice particles, the corresponding spatial distributions of electron density with small-scale structures are obtained, which may be one of the reasons of PMSE phenomenon.

Acknowledgements

The research has been financially supported by the National Natural Science Foundation of China under Grant Nos. 11775062 and 61601419.

REFERENCE

Allen J.: Probe theory-the orbital motion approach, Physica Scripta, 45, 497-503, 1992.

Antonsen T., Havnes O., Mann I.: Estimates of the Size Distribution of Meteoric Smoke Particles From Rocket‐Borne Impact Probes, Journal of Geophysical Research: Atmospheres, 122, 2017.

Bardeen C., Toon O., Jensen E., etc.: Numerical simulations of the three‐dimensional distribution of meteoric dust in the mesosphere and upper stratosphere, Journal of Geophysical Research: Atmospheres, 113, D17202, 2008.

Chilson P. B., Belova E., Rietveld M. T., etc.: First artificially induced modulation of PMSE using the EISCAT heating facility, Geophysical research letters, 27, 3801-3804, 2000.

Ecklund W., Balsley B.: Long‐term observations of the Arctic mesosphere with the MST radar at Poker Flat, Alaska, Journal of Geophysical Research: Space Physics, 86, 7775-7780, 1981.

Garcia R. R., Solomon S.: The effect of breaking gravity waves on the dynamics and chemical composition of the mesosphere and lower thermosphere, Journal of Geophysical Research: Atmospheres, 90, 3850-3868, 1985.

Havnes O., Pinedo Nava H., La Hoz C., etc.: A comparison of overshoot modelling with observations of polar mesospheric summer echoes at radar frequencies of 56 and 224 MHz, Annales Geophysicae, 33, 737-747, 2015.

Havnes O., Trøim J., Blix T., etc.: First detection of charged dust particles in the Earth's mesosphere, Journal of Geophysical Research: Space Physics, 101, 10839-10847, 1996.

Hill R., Gibson-Wilde D., Werne J., etc.: Turbulence-induced fluctuations in ionization and application to PMSE, Earth, planets and space, 51, 499-513, 1999.

Jensen E., Thomas G. E.: A growth‐sedimentation model of polar mesospheric clouds: Comparison with SME measurements, Journal of Geophysical Research: Atmospheres, 93, 2461-2473, 1988.

Johannessen A., Krankowsky D.: Positive‐ion composition measurement in the upper mesosphere and

lower thermosphere at a high latitude during summer, Journal of Geophysical Research, 77, 2888-2901, 1972.

Körner U., Sonnemann G.: Global three‐dimensional modeling of the water vapor concentration of the mesosphere‐mesopause region and implications with respect to the noctilucent cloud region, Journal of Geophysical Research: Atmospheres, 106, 9639-9651, 2001.

Khrapak S., Ratynskaia S. V., Zobnin A., etc.: Particle charge in the bulk of gas discharges, Physical Review E, 72, 016406, 2005.

Lübken F.-J., Lautenbach J., Höffner J., etc.: First continuous temperature measurements within polar mesosphere summer echoes, Journal of Atmospheric and Solar-Terrestrial Physics, 71, 453-463, 2009.

Lübken F. J.: Thermal structure of the Arctic summer mesosphere, Journal of Geophysical Research: Atmospheres, 104, 9135-9149, 1999.

Lübken F. J., Rapp M., Blix T., etc.: Microphysical and turbulent measurements of the Schmidt number in the vicinity of polar mesosphere summer echoes, Geophysical Research Letters, 25, 893-896, 1998.

Li H., Wu J., Zhou Z.: The formation of multiple layers of ice particles in the polar summer mesopause region, Annales Geophysicae, 34, 117-122, 2016.

Lie‐Svendsen Ø., Blix T., Hoppe U. P., etc.: Modeling the plasma response to small‐scale aerosol particle perturbations in the mesopause region, Journal of Geophysical Research: Atmospheres, 108, 8442, 2003.

Lieberman M. A., Lichtenberg A. J.: Principles of plasma discharges and materials processing, John Wiley & Sons, 2005.

Pedersen A., Troim J., Kane J.: Rocket measurements showing removal of electrons above the mesopause in summer at high latitude, Planetary & Space Science, 18, 945-947, 1970.

Pfaff R., Holzworth R., Goldberg R., etc.: Rocket probe observations of electric field irregularities in the polar summer mesosphere, Geophysical research letters, 28, 1431-1434, 2001.

Röttger J., La Hoz C., Kelley M. C., etc.: The structure and dynamics of polar mesosphere summer echoes observed with the EISCAT 224 MHz radar, Geophysical research letters, 15, 1353-1356, 1988.

Röttger J., Rietveld M., La Hoz C., etc.: Polar mesosphere summer echoes observed with the EISCAT 933‐MHz radar and the CUPRI 46.9‐MHz radar, their similarity to 224‐MHz radar echoes, and their relation to turbulence and electron density profiles, Radio Science, 25, 671-687, 1990.

Rapp M., Lübken F.-J.: Modelling of particle charging in the polar summer mesosphere: Part 1—General results, Journal of Atmospheric and Solar-Terrestrial Physics, 63, 759-770, 2001.

Rapp M., Lübken F.-J.: Polar mesosphere summer echoes (PMSE): Review of observations and current understanding, Atmospheric Chemistry and Physics, 4, 2601-2633, 2004.

Rapp M., Lübken F. J.: On the nature of PMSE: Electron diffusion in the vicinity of charged particles

revisited, Journal of Geophysical Research: Atmospheres, 108, 8437, 2003.

Reid G. C.: Ice particles and electron “bite‐outs” at the summer polar mesopause, Journal of Geophysical Research: Atmospheres, 95, 13891-13896, 1990.

390 Schunk R.: Mathematical structure of transport equations for multispecies flows, Reviews of Geophysics, 15, 429-445, 1977.

Seele C., Hartogh P.: Water vapor of the polar middle atmosphere: Annual variation and summer mesosphere conditions as observed by ground‐based microwave spectroscopy, Geophysical Research Letters, 26, 1517-1520, 1999.

395 Ullah S., Li H., Rauf A., etc. Case study of electron temperature effect on simultaneously observed VHF and UHF PMSE[C], In 2nd Asia-Pacific Conference on Plasma Physics. Kanazawa, Japan. 2018.